Available online at www.sciencedirect.com
ScienceDirect
Catalysis Today 131 (2008) 15–20
CATALYSIS TODAY
www.elsevier.com/locate/cattod

Rapid preparation of Bi_2WO_6 photocatalyst with nanosheet morphology via microwave-assisted solvothermal synthesis

Ling Wu [a,b], Jinhong Bi [a], Zhaohui Li [a], Xuxu Wang [a], Xianzhi Fu [a,*]

[a] *Research Institute of Photocatalysis, State Key Laboratory Breeding Base of Photocatalysis, Fuzhou University, Fuzhou 350002, PR China*

[b] *State Key Laboratory of Structural Chemistry, Fujian Institute of Research on the Structure of Matter, Chinese Academy of Sciences, Fuzhou 350002, PR China*

Available online 26 November 2007

Abstract

Nanocrystalline Bi_2WO_6 photocatalyst with nanosheet morphology was successfully synthesized by a microwave-solvothermal process. The prepared samples were characterized by X-ray diffraction technique (XRD), BET surface area analysis, Uv–vis diffuse reflectance spectrum (Uv–vis DRS), field emission scanning electron microscopy (SEM), transmission electron microscopy (TEM) and X-ray photoelectron spectroscopy (XPS). In comparison with a conventional hydrothermal process, the microwave-solvothermal process presented many advantages in a shorter reaction time, higher surface area and more oxygen vacancies for the preparation of Bi_2WO_6 samples. The absorption edge of the samples is at ca. 445 nm, corresponding to band gap energy of about 2.8 eV. The morphology of nanosheets with nanocrystals was also observed. For the decomposition of Rhodamine B (RhB) under visible light irradiation ($\lambda > 420$ nm), nanocrystalline Bi_2WO_6 samples obtained by microwave-solvothermal process showed higher photocatalytic activity than that of the sample obtained by conventional hydrothermal process.
© 2007 Elsevier B.V. All rights reserved.

Keywords: Microwave; Solvothermal; Bi_2WO_6; Nanosheet; Photocatalytic activity

1. Introduction

Bi_2WO_6 as an Aurivillius-phase perovskite belongs to the bismuth oxides family with a structure consisting of perovskite layers ($A_{m-1}B_mO_{3m+1}$) between bismuth oxide layers (Bi_2O_2) as shown in Fig. 1 [1–6]. The Bi_2O_2 layers are comprised of a square planar net of oxygen anions with the Bi^{3+} cations alternatively above and below the plane and can be described as forming caps of the BiO_4 square pyramids. This compound has been found to possess interesting physical properties such as ferroelectric piezoelectricity, pyroelectricity, catalytic behavior and a nonlinear dielectric susceptibility [7]. Recently, research into the use of Bi_2WO_6 as a visible-light-induced photocatalyst splitting water into H_2 and O_2 and decomposing the organic contamination has also attracted considerable interest [8–14]. Until now, solid-state reaction [13,14], amorphous complex precursor method [9], molten salt method [8] and hydrothermal process [10–12] have been employed to prepare Bi_2WO_6 photocatalyst, while the use of microwave-solvothermal process to synthesize this compound has not been reported.

It is reported that uniform nucleation and growth rates are critical to material quality. While for the most part, the synthetic methods utilize conventional convective heating due to the need for high-temperature initiated nucleation followed by controlled precursor addition to the reaction. But the convective heating can cause sharp thermal gradients throughout the bulk solution and inefficient, nonuniform reaction conditions [15]. In order to overcome this shortcoming, it is urged to search new approaches for synthesis. Microwave has been employed to address these problems. Microwaves are a portion of the electromagnetic spectrum with frequencies in the range of 0.3–300 GHz. The corresponding wavelengths of these frequencies are 1 m to 1 mm. The most commonly used frequency is 2.45 GHz. The degree of interaction of microwaves with a dielectric medium is related to the material's dielectric constant and dielectric loss [16]. When a material is polarized in an alternating field some energy is lost as heat. The fraction of energy lost during each reversal is the dielectric loss

* Corresponding author. Tel.: +86 591 83738608; fax: +86 591 83738608.
E-mail address: xzfu@fzu.edu.cn (X. Fu).

0920-5861/$ – see front matter © 2007 Elsevier B.V. All rights reserved.
doi:10.1016/j.cattod.2007.10.089

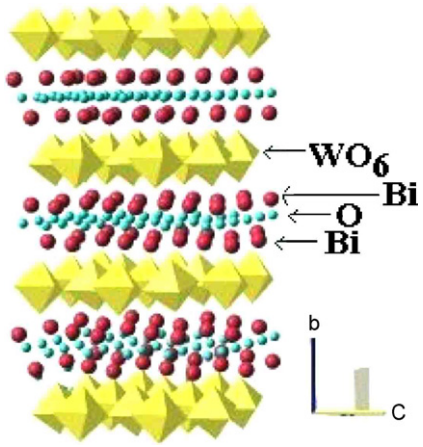

Fig. 1. Schematic structure of Bi_2WO_6.

[17]. Compared to the convection heating, microwave heating through dielectric losses is fast, simple, uniform, energy efficient and has been used in preparative chemistry and materials synthesis [18]. In addition, the microwaves may also be able to initiate chemical reactions not possible in conventional processing through selective heating of reactants and the new materials may be created [19]. Up to now, a lot of metal oxides have been synthesized by this method such as $CdIn_2S_4$ nanotubes [20], ZnS, CdS, CdSe [21], TiO_2 [22], $BiFeO_3$ [23] and so on.

In this paper, the microwave-solvothermal process was employed to synthesize the visible-light-induced photocatalyst Bi_2WO_6. It displayed a higher photocatalytic activity than the sample prepared by conventional hydrothermal process due to large Brunauer–Emmett–Teller (BET) surface area and the presence of more oxygen vacancy.

2. Experimental

2.1. Materials and sample preparation

$Bi(NO_3)_3{\cdot}5H_2O$ and $(NH_4)_{10}W_{12}O_{41}{\cdot}5H_2O$ were used as the starting materials for the syntheses, which are all A.R. grade reagents without further purification. In a typical process, 4 mmol $Bi(NO_3)_3{\cdot}5H_2O$ and 0.17 mmol $(NH_4)_{10}W_{12}O_{41}{\cdot}5H_2O$ were put into the 100 mL Teflon lined digestion vessel. Then 20 mL ethylene glycol was added. Under stirring, 5% $NH_3{\cdot}H_2O$ was dripped to adjust the pH to 9. The reaction mixture was sealed in the vessel by the vessel cover acting as an overpressure release valve. Then the vessel was surrounded by a safety shield and heated by a microwave synthesizer (ETHOS TC from Milestone Inc.) at 160 °C for different time. The processed time was 2 h and 4 h, respectively. Light yellow suspensions were formed after the microwave treatment. The products were washed by the deionized water and then dried at 80 °C before analysis.

As a comparison, conventional hydrothermal process was also used to synthesize Bi_2WO_6 nanosheets. In this process, the solvent was water instead of ethylene glycol and the reaction time was changed to 12 h compared to the microwave-solvothermal process.

2.2. Characterizations

The as-prepared samples were characterized by powder X-ray diffraction on a Bruker D8 Advance X-ray diffractometer at 40 kV and 40 mA with Ni filtered Cu Kα radiation. Data were recorded at a scan rate of 0.02° $2\theta\ s^{-1}$ in the 2θ range 20–80°. The crystallite size was calculated from X-ray line broadening via the Scherrer equation: $D = 0.89\lambda/\beta \cos\theta$, where D is the crystal size in nm, λ the Cu $K\alpha_1$ wavelength (1.5406 Å), β the half-width of the peak in radians and θ is the corresponding diffraction angle. Brunauer–Emmett–Teller surface area was measured by using ASAP2020M from Micromeritics Instrument Corporation. Uv–vis diffuse reflectance spectra (Uv–vis DRS) of the samples were obtained for the dry-pressed disk sample using a UV-visible spectrophotometer (Cary 500). $BaSO_4$ was used as a reflectance standard. Field scanning electron microscopy (SEM) was conducted on JSM-6700F. The transmission electron microscopy (TEM) and the high resolution transmission electron microscopy (HRTEM) images were taken by JEOL model JEM 2010 EX instrument at the accelerating voltage of 200 kV. The powder particles were supported on a carbon film coated on a 3 mm diameter fine-mesh copper grid. A suspension in ethanol was sonicated, and a drop was dripped on to the support film. X-ray photoelectron spectroscopy (XPS) measurements were carried out by using a VG Scientific ESCA Lab Mark II spectrometer equipped with two ultra-high vacuum 6 (UHV) chambers. All binding energies were referred to the C 1s peak at 284.8 eV of the surface adventitious carbon.

2.3. Photocatalytic activity measurements

The photocatalytic activities of Bi_2WO_6 were evaluated by the decomposition of RhB in an aqueous solution. 80 mg of catalyst was suspended in a 100 mL Pyrex glass vessel which contained 80 mL Rhodamine B (RhB) solution (10^{-5} mol/L). The light source was a 300 W halogen lamp (Philips Electronics), which was placed in a cylindrical glass vessel. Two cutoff filters were used to cutoff the light below 420 nm and above 850 nm to make sure the photoreaction went on under the visible light irradiation. The suspension was also stirred in the dark for 6 h to achieve the adsorption counterpoise. At given irradiation time intervals, 3 mL of the suspension was collected, and then centrifuged to remove the photocatalyst. The degraded solution was analyzed by a Varian Cary 50 Scan UV-visible spectrophotometer and the absorption peak at 554 nm was monitored.

Table 1
Preparation conditions, crystallite size and BET surface area of nanocrystal Bi_2WO_6 samples synthesized through a conventional hydrothermal (CH) route and microwave-solvothermal (MS) route

Sample	Treatment conditions	Crystallite size (nm)	BET (m^2/g)
S1	MS-160 °C 2 h	–	9.0
S2	MS-160 °C 4 h	30	10.6
S3	CH-160 °C 12 h	27	8.1

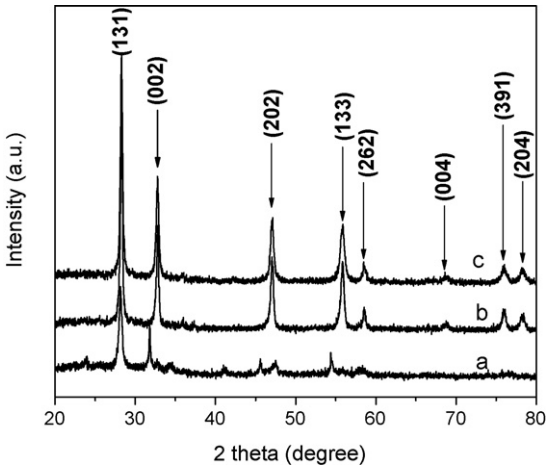

Fig. 2. XRD patterns of the samples: a: S1, b: S2 and c: S3.

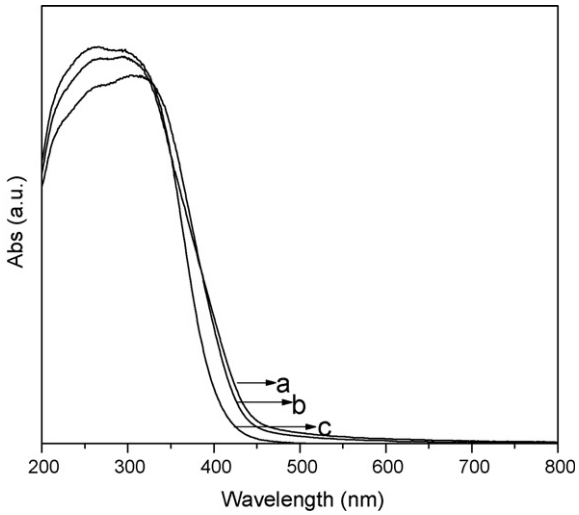

Fig. 3. UV–vis diffuse reflectance of the samples: a: S2, b: S3 and c: S1.

3. Results and discussion

3.1. XRD and Brunauer-Emmett-Teller (BET) surface area

The preparation conditions, crystallite size and BET surface area for samples S1–S3 are summarized in Table 1. The BET surface areas are 9.0 m^2/g, 10.6 m^2/g and 8.1 m^2/g, respectively, as shown in Table 1. Fig. 2 shows the phase analysis of the samples using XRD. Sample S1 (Fig. 2. curve a) shows a Bi_2WO_6 phase with other certain intermediates. When the

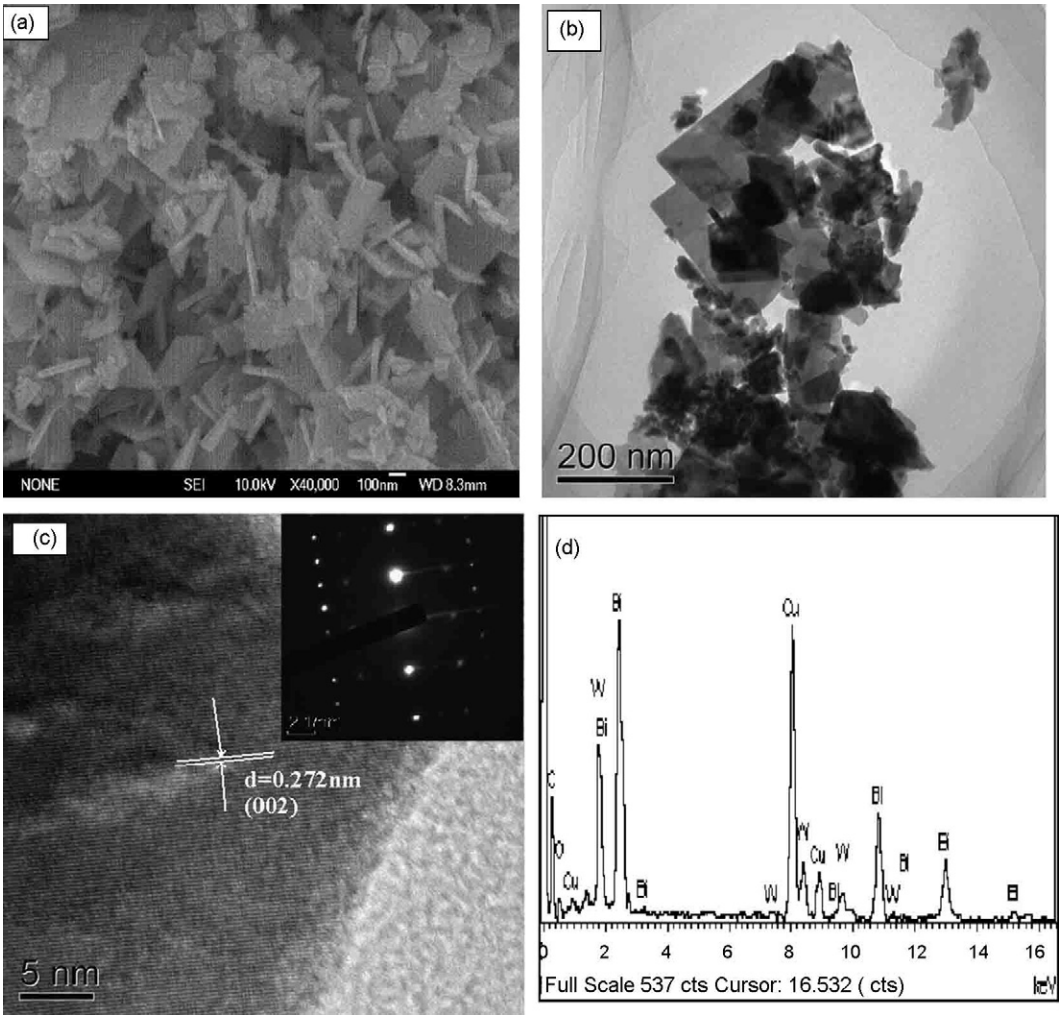

Fig. 4. The TEM images, HRTEM images and EDS spectrum of S2.

treatment time increases to 4 h (Fig. 2. curve b), the dominant peaks at 2θ of about 28.3°, 32.7°, 47.1°, 55.8°, 58.5°, 68.7°, 75.9° and 78.3° are observed. These peaks are indexed to crystalline structure of Russellite Bi_2WO_6 (JCPDS 79-2381), corresponding to the indices of (1 3 1), (0 0 2), (2 0 2), (1 3 3), (2 6 2), (0 0 4), (3 9 1), (2 0 4) planes, respectively. The similar features are found in sample S3 (Fig. 2, curve c). Compared to sample S3, sample S2 displays similar peaks intensity although its treatment time is far shorter than that of sample S3. This reveals that the use of microwave-solvothermal route can really obtain good quality crystals in a far shorter time.

3.2. Optical absorption of Bi_2WO_6 nanocrystal

Optical absorption of Bi_2WO_6 nanocrystals is measured by using a UV-vis spectrometer. Fig. 3 shows typical diffuse reflection spectra of all samples. The optical absorption of sample S2 and S3 is nearly the same. The wavelength at the absorption edge, λ, is determined as the intercept on the wavelength axis for a tangent line drawn on absorption spectra. The absorption for the samples locates at ca. 445 nm, corresponding to band gap energy of about 2.8 eV. As can be expected from the absorption spectra, the nanocrystals are yellow in color. Intense absorption bands with a steep edge in the visible light region are observed. These indicate that the visible light absorption band is induced by the band gap transition instead of the transition from impurity levels [24].

3.3. Morphology of Bi_2WO_6 nanocrystal

The evolution of the particle size and morphologies of sample S2 synthesized by microwave-solvothermal route is clearly revealed by SEM image in Fig. 4a. It shows that the products consist of a large quantity of nanosheets with some nanocrystallites. The morphology is also confirmed by TEM image (Fig. 4b). The HRTEM image (Fig. 4c) shows clear lattice fringes. The fringes of $d = 0.272$ nm match that of the (0 0 2) crystallographic plane of Bi_2WO_6. A typical SAED pattern (inset of Fig. 3c) shows the single-crystalline structure of the nanosheet. Fig. 4d shows EDS pattern recorded in TEM. The result from EDS displays that the sample contains Bi, W, Cu and O elements. The element of Cu is from the Cu grid.

3.4. XPS

X-ray photoelectron spectroscopy surface measurements are performed on Bi_2WO_6 powders to determine the elemental composition and oxidation state. Fig. 5 shows the Bi 4f, W 4f, O

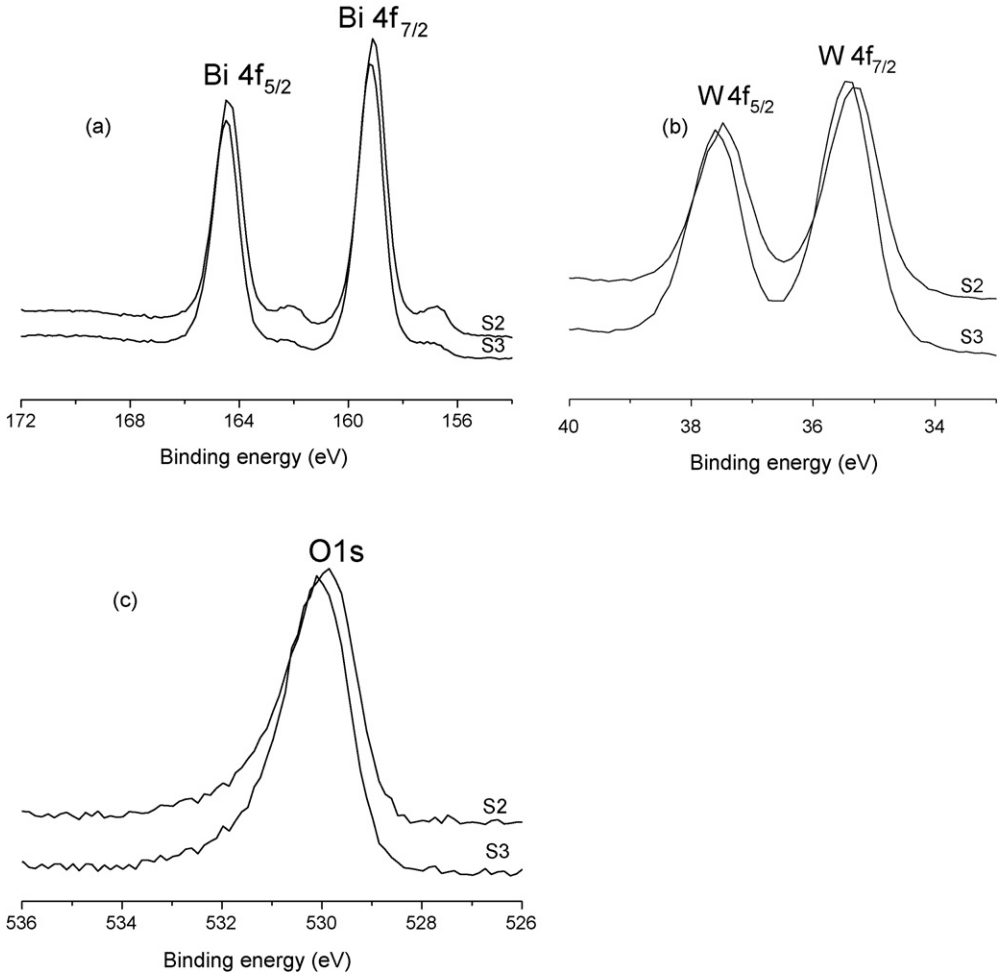

Fig. 5. High resolution XPS spectra of the nanocrystalline Bi_2WO_6: a: Bi 4f, b: W 4f and c: O 1s.

1s XPS peaks for samples S2 and S3. Characteristic binding energy (BE) value of 159.1 eV for Bi $4f_{7/2}$ (Fig. 5a) reveals a trivalent oxidation state for bismuth. An additional spin–orbit doublet with binding energy of 156.8 eV for Bi $4f_{7/2}$ is also observed in sample S2. It suggests that some parts of bismuth exist in the $(+3-x)$ valence state. This means that the trivalent bismuth is partly reduced to the lower valence state in the microwave-solvothermal process (S2). The ethylene glycol may serve as both a solvent and a reductant under the microwave irradiation [25]. The similar chemical shift of about 2.3 eV for Bi $4f_{7/2}$ was also observed by Jovalekic et al. [26]. They concluded that this shift suggesting the Bi $(+3-x)$ formal oxidation state could most probably be attributed to the substoichiometric forms of Bi within the Bi_2O_2 layer. The production of low oxidation state results in the existence of oxygen vacancy. For sample S3, the contribution of the additional doublet is less apparent. It indicates that bismuth with low oxidation state is negligible in sample S3. In other words the amount of oxygen vacancies in sample S2 is more than that in sample S3. As the oxygen vacancies are caused by the charge balance, it seems there is no relationship between oxygen vacancy and crystallinity. The binding energy at 37.5 eV and 35.4 eV for W $4f_{5/2}$ and W $4f_{7/2}$ (Fig. 5b) can be assigned to a W^{6+} oxidation state [27]. As shown in Fig. 5c the O element may be fitted into two kinds of chemical states: crystal lattice oxygen and adsorbed oxygen [28].

3.5. Photocatalytic activity evaluation

Photocatalytic activities of the samples are evaluated by the degradation of Rhodamine B in the aqueous solution under visible light irradiation. Temporal changes in the concentration of RhB are monitored by examining the variations in maximal absorption in UV–vis spectra at 554 nm. Fig. 6 displays the concentration changes of Rhodamine B at 554 nm as a function of irradiation time during the degradation process in aqueous Bi_2WO_6. Samples S2 and S3 show a far higher photocatalytic activity than that of sample S1 which affirms that the photocatalytic activity is really induced by the Bi_2WO_6. Fig. 7a and b shows the temporal evolution of the spectral changes of the RhB mediated by S2 and S3, respectively. With the photocatalytic degradation of RhB, the absorption peak at 554 nm blue-shifts and turns broadened at the same time. This agrees well with the report of Zhao and coworkers in the TiO_2/RhB process [29–30]. According to their report, the blue-shift of absorption band is caused by de-ethylation of RhB because of the attack by one of the active oxygen species on the *N*-ethyl group. When the de-ethylated process is fully completed, the absorption band shifts to 498 nm at wavelength and RhB turns to rhodamine. Then rhodamine is gradually decomposed due to the further destruction of the conjugated structure. Moreover, the different decomposed processes of RhB are observed in Fig. 7a and b. Fig. 7a for sample S2 presents a slower change in de-ethylation of RhB with concomitance of a rapid destruction of the conjugated structure. However, Fig. 7b for sample S3 shows a rapid process in de-ethylation of RhB and then the slower destruction of the conjugated structure. It can be observed that after RhB turns to rhodamine sample S2 shows a relatively higher photocatalytic activity which may be contributed to the relatively large surface area, and the presence of more oxygen vacancies affirmed by XPS [31].

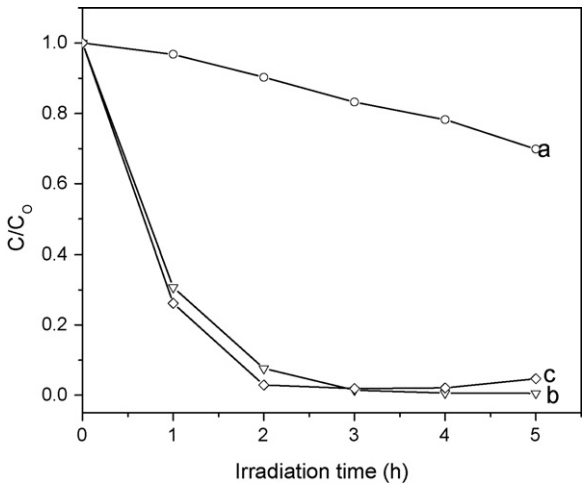

Fig. 6. Concentration changes of Rhodamine B at 554 nm as a function of visible light irradiation time in the presence of photocatalysts; $\lambda > 420$ nm; a: S1, b: S2 and c: S3.

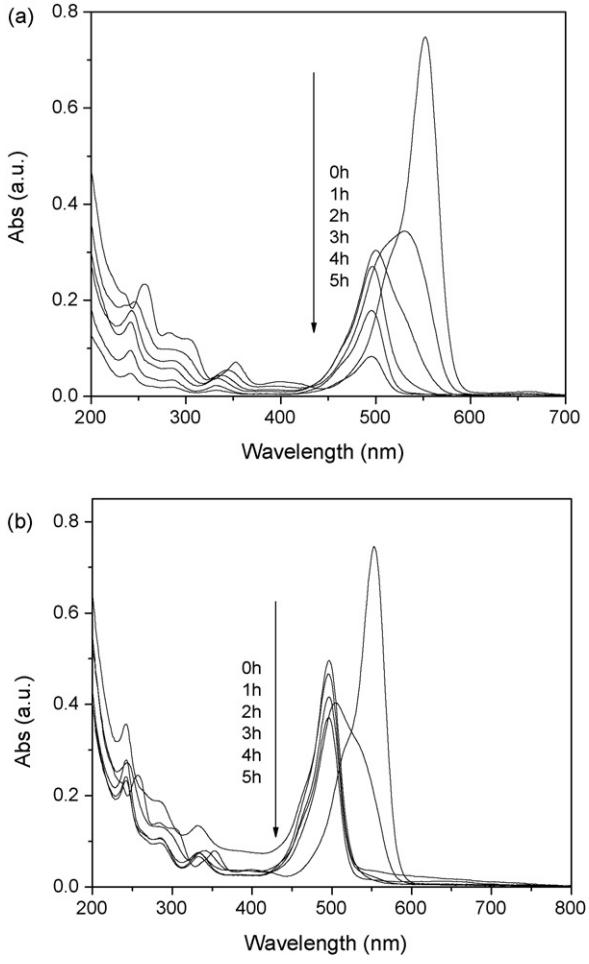

Fig. 7. UV–vis spectral changes of RhB (10^{-5} M) in aqueous Bi_2WO_6 (a: S2 and b: S3) dispersions as a function of irradiation time.

4. Conclusions

Nanocrystalline Bi_2WO_6 photocatalyst with visible-light response is successfully synthesized by the microwave-solvothermal route. The results show that the prepared sample has high surface area and small crystallite size. The Uv–vis DRS exhibits strong visible light absorption at ca. 445 nm for all prepared samples, corresponding to band gap energy of about 2.8 eV. SEM and TEM images present the morphology with nanosheets and nancrystals for sample S2. The photocatalytic evaluation, via the decomposition of Rhodamine B (RhB) under visible light irradiation ($\lambda > 420$ nm), reveals that nanocrystalline Bi_2WO_6 samples obtained in different condition exhibit different photocatalytic performances. The photocatalytic activities are mainly affected by specific surface area and oxygen vacancy.

Acknowledgments

This work was financially supported by the National Natural Science Foundation of China (20571015, 20573020, 20777011 and 20537010), the National High Technology Research and Development Program of China (863 project 2006AA03Z340), National Basic Research Program of China (973 Program: 2007CB613306) and the Natural Science Foundation (E0510011) and the Scientific Project of Fujian Province, China (2005HZ1008 and 2005K002).

References

[1] R.E. Newnmam, R.W. Wolfe, J.F. Dorrian, Mater. Res. Bull. 6 (1971) 1029.
[2] J.L. Hutchison, J.S. Anderson, C.N.R. Rao, Proc. R. Soc. Lond., Ser. A 355 (1977) 301.
[3] Y. Bando, A. Watanabe, Y. Sekikawa, M. Goto, S. Horiuchi, Acta Crystallogr. Sect. A 35 (1979) 142.
[4] B. Frit, J.P. Mercorio, J. Alloys Compd. 188 (1992) 27.
[5] M.T. Montero, P. Millan, P. Duran-Martin, B. Jimenez, A. Catro, Mater. Res. Bull. 33 (1998) 1103.
[6] A. Watanabe, M.J. Goto, Less-Common Met. 61 (1978) 265.
[7] Y. Shi, S. Feng, C. Cao, Mater. Lett. 44 (2000) 215.
[8] A.P. Finlayson, V.N. Tsaneva, L. Lyons, M. Clark, B.A. Glowacki, Phys. Status Solidi A: Appl. Mater. 203 (2006) 327.
[9] S.C. Zhang, C.A. Zhang, Y. Man, Y.F. Zhu, J. Solid State Chem. 179 (2006) 62.
[10] H.B. Fu, C.S. Pan, W.Q. Yao, Y.F. Zhu, J. Phys. Chem. B 109 (2005) 22432.
[11] J.G. Yu, J.F. Xiong, B. Cheng, Y. Yu, J.B. Wang, J. Solid State Chem. 178 (2005) 1968.
[12] C. Zhang, Y.F. Zhu, Chem. Mater. 17 (2005) 3537.
[13] J.W. Tang, Z.G. Zou, J.H. Ye, Catal. Lett. 92 (2004) 53.
[14] A. Kudo, S. Hijii, Chem. Lett. (1999) 1103.
[15] J.A. Gerbec, D. Magana, A. Washington, G.F. Strouse, J. Am. Chem. Soc. 127 (2005) 15791.
[16] W.H. Sutton, Am. Ceram. Soc. Bull. 68 (1989) 376.
[17] E. Siores, D. Do Rego, J. Mater. Process. Technol. 48 (1995) 619.
[18] S.A. Galema, Chem. Soc. Rev. 26 (1997) 233.
[19] E.T. Thostenson, T.W. Chou, Composites: Part A 30 (1999) 1055.
[20] B.B. Kale, J.O. Baeg, S.M. Lee, H. Chang, S.J. Moon, C.W. Lee, Adv. Funct. Mater. 16 (2006) 1349.
[21] A.B. Panda, G. Glaspell, M.S. EI-Shall, J. Am. Chem. Soc. 128 (2006) 2790.
[22] G.J. Wilson, G.D. Will, R.L. Frost, S.A. Montgomery, J. Mater. Chem. 12 (2002) 1787–1791.
[23] S. Komarneni, V.C. Menon, Q.H. Li, R. Roy, F. Ainger, J. Am. Ceram. Soc. 79 (1996) 1409.
[24] A. Kudo, I. Tsuji, H. Kato, Chem. Commun. (2002) 1958.
[25] R. Harpeness, A. Gedanken, New J. Chem. 27 (2003) 1191.
[26] C. Jovalekic, M. Pavlovic, P. Osmokrovic, L. Atanasoska, Appl. Phys. Lett. 72 (1998) 1051.
[27] J.H. Ryu, et al. J. Alloys Compd. 441 (2007) 146.
[28] L.Q. Jing, X.J. Sun, B.F. Xin, B.Q. Wang, W.M. Cai, H.G. Fu, J. Solid State Chem. 177 (2004) 3375.
[29] T. Wu, G. Liu, J. Zhao, J. Phys. Chem. B 102 (1998) 5845.
[30] W. Zhao, C. Chen, X. Li, J. Zhao, J. Phys. Chem. B 106 (2002) 5022.
[31] G. Lu, A. Linsebigler, J.T. Yates, J. Phys. Chem. 99 (1995) 7626.